Acta Cryst. (1983). A**39**, 211–216

Diffractometry and Reflection Profiles of Anisotropic Mosaic and Split Crystals

BY ALBERT J. M. DUISENBERG

Laboratorium voor Structuurchemie, Rijksuniversiteit Utrecht, Padualaan 8, 3584 *CH Utrecht, The Netherlands*

(*Received* 20 *July* 1982; *accepted* 6 *October* 1982)

Abstract

Both anisotropic mosaicity and splitting of a crystal is described by means of a 'rotational cluster' model with a predominant rotation about a vector **A**. Procedures are outlined to obtain **A** from intensity scans made at different orientations about the diffraction vector, and to compute for all reflections those diffractometer setting angles for which the effect from anisotropy or splitting upon the profile is minimal. The relevant Fortran programs, *ANIVEC* and *ANIMO*, for our Enraf–Nonius CAD4F four-circle diffractometer system are available.

Introduction

Methods to obtain net intensities with a single-crystal diffractometer can be divided into two categories: 'non-profile' and 'profile' methods. Examples of non-profile methods are background–peak–background (BPB) methods and peak intensity measurements; examples of profile methods are curve fitting (*e.g.* Clegg, 1981) and deconvolution and reconstruction methods (*e.g.* Nelmes, 1975).

In Fig. 1 two reflection profiles, (*a*) and (*b*), are displayed, both obtained from the same reflection of the same crystal. Profile (*a*) is not suited to profile methods; nor is it ideal for non-profile methods. The scan angle in the BPB method must be about twice as large for profile (*a*) as for (*b*), and it will certainly be impossible to produce reliable results with peak measurements. If alternatives (*a*) and (*b*) are available, obviously (*b*) is preferable.

In this paper a procedure based upon a simple model is proposed which can often be applied to obtain neat profiles.

Fig. 1 refers to a split crystal; with an anisotropic mosaic crystal the difference between the best and the worst profile of a reflection is less spectacular, but it is still worth using the proposed method because it leads to the narrowest profile for all reflections and minimizes the anisotropy in relation to the scan parameters. Important consequences for the aperture dimensions are discussed later, under *Remarks* (*a*) and (*b*).

0567-7394/83/020211-06$01.50

Splitting, mosaicity and the vector A

Consider a crystal consisting of two fragments, (1) and (2), which differ *slightly* in orientation. Associated with such a 'split' crystal we can specify three identical but differently orientated reciprocal lattices with reciprocal vectors **H**(1), **H**(2) and **H**, respectively, **H**(*i*) being the vector of fragment (*i*) and **H** the mean vector located between **H**(1) and **H**(2). We will restrict ourselves to the situations where all pairs **H**(1) and **H**(2) include such a small angle that the reflections **H**(1) and **H**(2)

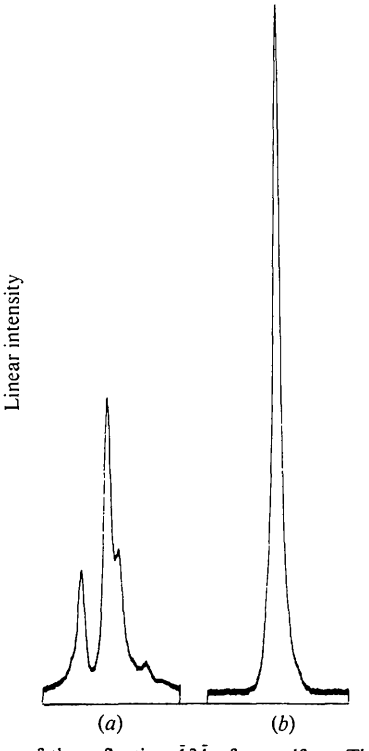

Fig. 1. ω scans of the reflection $\bar{1}3\bar{1}$ of acesulfam. The difference between the azimuth ψ for profiles (*a*) and (*b*) is 90°. Scan parameters: $\Delta\omega = 3°$; aperture width 1·95° and height 1·99°, as seen from the crystal. Mo radiation (Zr-filtered), $\theta = 7{\cdot}50°$. Note that for a BPB scan the $\Delta\omega$ value of 3° still is not sufficient for profile (*a*); the background level of (*b*) is not reached yet. From (*a*) it can be concluded that the crystal consists of at least four fragments and that it is anisotropic mosaic; comparing the outer parts of (*a*) and (*b*), one notes the effect of anisotropic mosaicity.

partially overlap so that diffractometer setting angles derived from vector **H** are sufficiently accurate to observe the reflections **H**(1) and **H**(2).

As the fragments are rigid bodies their relative orientation and that of the corresponding reciprocal lattices can be described by one rotation around some axis **A**. [From Chasle's theorem; see, for example, Goldstein (1959).] This means that the orientations of the vectors **H**(1) and **H**(2) are related by a rotation ε (Fig. 2*a*). The value of ε is the same for all reflections, and all rotations are about the same **A**. Then, to a good approximation,

$$\mathbf{A} \times \mathbf{H}(1) = \mathbf{H}(2) - \mathbf{H}(1),$$

apart from a constant which is of no importance here. Since ε is small, we replace **H**(1) on the left-hand side by **H** and substitute for **H**(2) − **H**(1) a vector **L** equal to [**H**(2) − **H**(1)]/|**H**(2) − **H**(1)|, so that |**L**| = 1. Then

$$\mathbf{A} \times \mathbf{H} = \mathbf{L},$$

again apart from a constant. This we call the '**A** model' for the splitting of a crystal: at the endpoint of each vector **H** a vector **L** of unit length is attached perpendicular to both **H** and **A**, in the direction of **H**(2) − **H**(1). The model is depicted in Fig. 2(*b*) for an arbitrary **H**.

To observe reflection **H** on a diffractometer the vector **H** is brought into the reflecting position in the horizontal plane. The orientation of **L** can be varied by ψ rotation about **H**, Fig. 5. In a 'ψ scan', *i.e.* a series of ω scans at different values of ψ, the effect of the orientation of **L** upon the profile is shown in Fig. 3, the narrowest profile occurring when **L** is vertical, the broadest when **L** is horizontal. Apart from mechanical limitations there are two values of ψ for which **L** is vertical, ψ_0 and $\psi_0 + 180°$. The values for which the profile is broadest are therefore $\psi_0 \pm 90°$.

A crystal consisting of more than two fragments and an anisotropic mosaic crystal can be described with the **A** model, when there is one predominant rotation relating the orientation of the crystal parts. Actually, there is no sharp division between the two types; they both could be considered as special cases of (dis)-continuously (an)isotropic mosaic crystals. It is our experience (with organic and organo-metallic compounds), firstly, that (dis)continuously anisotropic mosaicity is far from exceptional and, secondly, that the **A** model often fits such crystals, *i.e.* in reciprocal space the reflection domains are (dis)continuously elongated, perpendicular to a common axis, which is **A**. (We explicitly do not include the effects of wavelength dispersion, crystal size and source width.) Then, in the limiting cases, the domain is an ellipse (single crystal, anisotropic mosaic) or a row of circular dots (fragmented crystal, isotropic mosaic). In practice both features may be observed on the same crystal (as is the case with the crystal from Fig. 1). Fig. 2 is suited for visualizing the general situation. Vector **L** is defined by the elongation of the domain, and the angle ε quantifies the anisotropy and/or the splitting. (All **L** are samples, taken at **H**, from a rotational vector field with **A** as the rotation: **rot L** = **A**; this is an alternative representation of the **A** model.) It appears likely that the mechanisms causing fragmentation and anisotropy often results in (or is) a torsion.

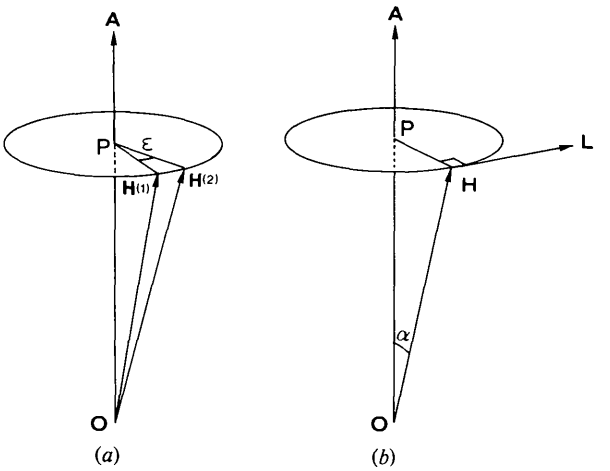

Fig. 2. (*a*) Illustration of the relation between the reciprocal vectors **H**(1) and **H**(2); **H**(1) and **H**(2) belong to crystal fragments (1) and (2) respectively and have the same indices. The orientations of **H**(1) and **H**(2) are related by a rotation ε about **A**; ε is the same for all pairs **H**(1) and **H**(2). The vector **H** in (*b*) corresponds to **H**(1) and **H**(2) when $\varepsilon = 0$. **H** is taken between **H**(1) and **H**(2) (not shown in *a*). The vector **L**, of unit length, points in the direction of **H**(2) − **H**(1) and is perpendicular to both **A** and **H**. In the reflecting position **H** is horizontal. The angular separation of **H**(1) and **H**(2) in the reflection profile (measured as a $\Delta\omega$) varies, with ψ, from zero (with **L** vertical) to $\varepsilon \sin \alpha$ (with **L** horizontal). (α is the angle between **H** and **A**.) Uniaxial anisotropic mosaicity can be treated in the same way: here the angular separation mentioned before is the *extra* width of the reflection due to anisotropy. With **L** vertical the basic component contributes to the reflection width and the anisotropic part to the vertical dimension of the reflection.

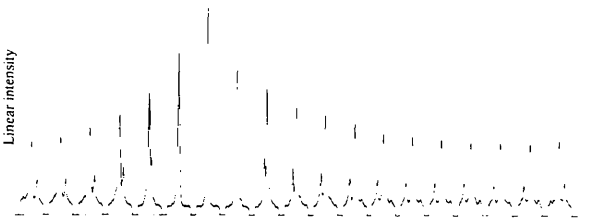

Fig. 3. A series of ω scans at different azimuth (a 'ψ scan') for the reflection $1\bar{3}\bar{3}$ of acesulfam. $\Delta\psi$ between the profiles is 10°, starting, on the *right*, with $\psi = -90°$ (that profile is scanned in the reverse sense). Scan parameters: $\Delta\omega = 3°$; aperture width 1·95° and height 0·99°, as seen from the crystal. Mo radiation (Zr-filtered), $\theta = 9{\cdot}58°$. From these scans ψ_0, ψ for the best profile, is chosen as 30°. The equivalent ψ_0 of 30 + 180 = 210° is out of reach of the instrument for this reflection: likewise only one broadest reflection can be shown, at ψ about 60°.

Not all types of splitting and mosaicity can be described by the simple **A** model, for instance twinning where the subreflections have *different* indices (Tichý & Beneš, 1979), or mosaicities with *two* preferred rotations (Rieck, 1971). Whether the crystal under investigation can rightly be treated as a 'rotational cluster' or not is decided in the procedure to find and establish **A**.

Calculation of A

We use a Cartesian coordinate system X,Y,Z defined in Appendix A and shown in Fig. 4. The components of **L** associated with reflection **H** are calculated from the observed ψ_o (= ψ for the best profile) and the bisecting setting angles φ and χ as (Appendix A)

$$\left.\begin{aligned} L_x &= \sin\chi \sin\varphi \cos\psi_o - \cos\varphi \sin\psi_o \\ L_y &= -\sin\chi \cos\varphi \cos\psi_o - \sin\varphi \sin\psi_o \\ L_z &= \cos\chi \cos\psi_o \end{aligned}\right\}. \quad (1)$$

In the same way we obtain from another reflection, **H'**, a vector **L'**. In the **A** model all vectors **L** are perpendicular to **A**, so we find **A** from

$$\mathbf{A} = \mathbf{L} \times \mathbf{L}'. \quad (2)$$

With more than two reflections, say n, we can form $P = n(n-1)/2$ different pairs $[\mathbf{L},\mathbf{L}']_i$, each of which gives a vector $\mathbf{A}_i$ ($i = 1, 2, \ldots, P$) with (2). For the resultant **A** we take

$$\mathbf{A} = \sum_i (\pm\mathbf{A}_i), \quad (3)$$

where the signs are chosen in such a way that all $\mathbf{A}_i$ point in the same direction ($|\mathbf{A}|$ is maximal). As all $|\mathbf{L}|$ are 1, $|\mathbf{A}_i|$ is equal to the sine of the angle between **L** and **L'**. The direction of $\mathbf{A}_i$ is more sensitive to directional errors of **L** and **L'** as the value of the corresponding sine is smaller. By using (3), the $\mathbf{A}_i$ that are less reliable contribute less to the direction of **A**. (An alternative method is to calculate by least squares the best plane through the origin and parallel to all **L**. The normal is the desired **A**. The result is the same.)

Calculation of ψ_o from A

Once **A** is known we can compute ψ_o for an arbitrary reflection **H** as follows. When **H** is in the reflecting position and $\psi = \psi_o$, then **L** is vertical. As **L** is always perpendicular to both **H** and **A** it follows that **A** is horizontal when $\psi = \psi_o$. This leads to (Appendix B)

$$\tan\psi_o = [(A_x \sin\varphi - A_y \cos\varphi)\sin\chi + A_z \cos\chi]/(A_x \cos\varphi + A_y \sin\varphi), \quad (4)$$

where φ and χ are the bisecting setting angles corresponding to the reflection **H**.

We can thus check whether the **A** model fits the crystal, first by comparing the observed and the calculated ψ_o for the reflections used to obtain **A**, secondly by observing the profiles of several other reflections at their calculated ψ_o (or at $\psi_o + 180°$ which is equivalent in this respect).

An example

All profiles and calculations refer to a crystal of 'acesulfam' [6-methyl-1,2,3-oxathiazin-4(3*K*)-one 2,2-dioxide; Paulus, 1975]. From six reflections, ψ scans were recorded with $\Delta\psi = 10°$ (Fig. 3 is such a scan). The value of ψ_o(obs) is given in Table 1; it is the ψ value for the best profile of the ψ scan; no attempt was made to obtain more accurate values by using interpolation or other methods. The six reflections form 15 pairs from which vectors $\mathbf{A}_i$ are calculated, indicated as $\mathbf{A}(n,n')$ in Table 2. We have written a program *ANIVEC* for the Enraf–Nonius CAD4F, but the calculations are so simple that they can easily be performed on a programmable pocket calculator to experiment with the method first. *ANIVEC*, which

Table 1. *Observed and calculated azimuth for the best profiles, ψ_o(obs) and ψ_o(calc), respectively*

ψ_o(calc) are the results obtained by using the reflections numbered 1 through 6; ψ_o(calc,2) is obtained by using only two reflections, marked with *.
The vectors **L**, given as components in X,Y,Z (Appendix A), are obtained with formula (1) from ψ_o(obs) and the bisecting setting angles φ and χ. They are referred to in Table 2.

n	h	k	l	ψ_o(obs)	ψ_o(calc)	ψ_o(calc,2)	φ	χ	$L_x(n)$	$L_y(n)$	$L_z(n)$
1*	−3	−3	3	−25	−22·5	−25·0	−146·88	36·43	−0·648	0·220	0·729
2	−2	4	−2	−70	−67·3	−62·2	−0·85	34·28	0·937	−0·207	0·283
3*	−2	4	−3	−50	−55·4	−50·0	8·76	35·44	0·814	−0·252	0·524
4	−1	−3	−5	15	16·8	22·2	108·71	35·15	0·610	−0·067	0·790
5	−1	−2	−5	10	10·4	15·4	97·69	37·45	0·617	−0·092	0·782
6	−3	−5	1	−60	−59·6	−59·7	−177·97	39·04	−0·877	0·284	0·388
	−1	3	−1	−60	−68·8	−63·1	−5·63	24·11			
	−1	−3	−3	30	32·4	37·0	124·90	36·37			
	−3	−1	4	0	−2·2	−4·3	−117·29	32·24			
	−4	0	−1	70	74·1	75·6	−32·11	85·05			

needs the cell and orientation matrix, accepts from two to nine reflections, for which the indices and ψ_o should be given; it performs the calculations as given in (1) and computes all possible $\mathbf{A}_i$ with (2). The output is seen in Table 2, from which it can be concluded that, in this example, the **A** model fits reasonably well, taking into account the fact that the ψ_o(obs) were rather crudely determined. Of practical importance especially is the agreement between ψ_o(obs) and ψ_o(calc) (Table 1), obtained from the final **A** with (4) (which is part of our subroutine *ANIMO* on the CAD4). Here the hypothesis that the **A** model fits this crystal is corroborated. Our principal purpose, *i.e.* to obtain profiles as in Fig. 1(*b*), is attained sufficiently closely with these values of ψ_o(calc).

It is possible, in principle, to calculate **A** from two reflections. In Table 1, the column ψ_o(calc,2) gives the results when only the reflections numbered 1 and 3 are used. Vector **A** is **A**(1,3) from Table 2. A satisfying result can only be expected with a not too small angle between the vectors **L** and **L**′ (formula 2); the sine of this angle appears in the column 'sin' in Table 2. The results are not conclusive without comparing ψ_o(obs) and ψ_o(calc) for *other* reflections.

From comparison of the two bottom lines in Table 2 it is evident that **A** is near the (monoclinic) *b* axis. The situation that the vector **A** is perpendicular to a crystal plane with low indices [here (010)] is met frequently; this is in accord with the assumption that fragmentation and anisotropy can often be considered as a torsion.

In the data-collecting program, the subroutine *ANIMO* calculates ψ_o. The actual azimuth ψ at which a reflection is measured is determined either by

$$\psi = \psi_o \pm n \times 10°$$

or by

$$\psi = (\psi_o + 180°) \pm n \times 10°$$

depending on which formula gives the smallest n (n is a natural number), taking mechanical obstructions into account. From 6660 reflections (all reflections in the Mo sphere with $\theta < 27{\cdot}5°$), n was 0, 1, 2, 3, 4 for 6215, 200, 146, 88 and 11 reflections, respectively. Inspection of Fig. 3 establishes that a difference of 10° between ψ and ψ_o is not very harmful so in this case we were able to measure 96% of the reflections with a decent profile.

Table 2. *Vectors* **A**(*n*,*n*′), *given as components in X,Y,Z (Appendix A), as obtained from vectors* **L**(*n*) *and* **L**(*n*′) *with formula* (2)

The **A**(*n*,*n*′) are given in normalized form (length = 1). Their true length, and hence their contribution to **A**(final), is given in the column 'sin'; 'sin' is the sine of the angle between the corresponding **L**(*n*) and **L**(*n*′). The numbers *n* and *n*′ refer to column *n* in Table 1. **A**(final) is calculated with formula (3). The column $\Delta°$ gives the angle with **A**(final). Note that a more deviating **A**(*n*,*n*′) contributes less to **A**(final), by its smaller 'sin'.
From the last line it can be concluded that **A**(final) is (practically) along the *b* axis.

A(*n*,*n*′)	*x*	*y*	*z*	sin	$\Delta°$
A(1,2)	0·238	0·968	−0·080	0·895	2·6
A(1,3)	0·305	0·952	−0·016	0·980	5·2
A(1,4)	0·226	0·971	−0·092	0·986	1·4
A(1,5)	0·242	0·968	−0·077	0·989	1·3
A(1,6)	0·300	0·953	−0·022	0·407	5·1
A(2,3)	0·136	0·960	−0·250	0·272	11·6
A(2,4)	0·246	0·964	−0·107	0·589	0·9
A(2,5)	0·236	0·969	−0·073	0·576	2·9
A(2,6)	0·252	0·959	−0·133	0·638	2·3
A(3,4)	0·433	0·852	−0·261	0·376	16·6
A(3,5)	0·419	0·879	−0·228	0·356	12·2
A(3,6)	0·303	0·952	−0·012	0·814	5·8
A(4,5)	0·741	0·370	−0·556	0·027	52·5
A(4,6)	0·258	0·960	−0·118	0·969	2·0
A(5,6)	0·267	0·959	−0·098	0·965	0·5
A(final)	0·273	0·957	−0·095	–	0·0
b axis	0·279	0·957	−0·083	–	0·8

Remarks

(*a*) The ψ scan consists of a series of ω-scan profiles of the same reflection with $\Delta\psi = 10°$ between the settings. The scan angle, $\Delta\omega$, and the aperture dimensions are not so critical as in data collection; they merely should be chosen not too small. The aperture height should be considered especially, because at $\psi = \psi_o$ all the effect of anisotropy and splitting enters the vertical dimension of the reflection across the aperture. The 'best profile' of the ψ scan ($\psi = \psi_o$) is not automatically the highest one since absorption may interfere.

(*b*) The '*vertical* mosaicity' for the setting $\psi = \psi_o$ can be obtained from the *horizontal* profile width at $\psi = \psi_o \pm 90°$, by subtracting (deconvoluting) the broadening effects of wavelength dispersion, crystal size and source width. The vertical mosaicity thus found should be used in formulae as given by Alexander & Smith (1962) to calculate the slit height, when using the $\psi = \psi_o$ setting in data collection. This mosaicity is not the same for all reflections but proportional to sin α, α being the angle between **H** and **A**, as can be deduced from Fig. 2. In this context we observe that a controllable aperture height is at least as desirable as a variable slit width.

When, in data collection, all reflections are measured in the bisecting mode (*i.e.* $\psi = 0$) some, by chance, will be measured near ψ_o, some near $\psi_o \pm 90°$ and most somewhere in-between. This implies that one is confined to a large ω scan (because of the reflections near $\psi_o \pm 90°$) *and* to the aperture *height* accommodating the vertical mosaicity (ψ near ψ_o) as discussed above. (The use of an $\omega/2\theta$ scan would imply a large aperture *width* besides.) With the **A** method the aperture *height* is the same as with the bisecting mode, but the scan mode and aperture *width* can be chosen. Nevertheless,

one might prefer the $\psi_0 \pm 90°$ setting, *e.g.* when, in case of anisotropic mosaicity, the advantages of the narrow profile should not outweigh the disadvantages of secondary extinction at ψ_0 (as kindly pointed out by a referee). This requires only one minor change in the programming.

(*c*) The reflections to produce the ψ scans should be chosen to sample reciprocal space. If a reflection shows much less variation than the others (**H** near **A**) then it should be replaced.

(*d*) **A** can be found even if the true cell and orientation matrix is not known: Take a suitable triplet of non-coplanar **H**, use these as basis vectors and proceed with broken indices for the other reflections for the time being. This procedure can be useful when the 'subreflections' **H**(*i*) are too close to each other to be centered separately. Centering at ψ_0 may give better results than at $\psi = 0$, generally, certainly when the combined results of **H** at positive and $-$**H** at negative θ are used. The ω profiles both will have one maximum and the intensity distribution in the vertical direction across the aperture for **H** is that for $-$**H** upside down. We did meet cases, when this procedure was not used, where indexing was impossible.

(*e*) For *twinning* other methods are available (Tichý & Beneš, 1977). The **A** method may be helpful for analysis: when the reflection splitting can be totally removed by using **A**, twinning is almost certainly not the case.

APPENDIX *A*

We use CAD4 geometry; for other systems (the appropriate) changes in trigonometric functions should be made.

The Cartesian coordinate system X,Y,Z is attached to the diffractometer with its origin at the eucentric point (crystal), the Z axis vertically upward and the X axis pointing to the X-ray source (Fig. 4). With all settings at zero, the bisecting setting angles φ and χ for a reflection normal **H** are defined by

$$\sin \chi = H_z/(H_x^2 + H_y^2 + H_z^2)^{1/2}$$

$$\sin \varphi = -H_x/(H_x^2 + H_y^2)^{1/2}$$

$$\cos \varphi = H_y/(H_x^2 + H_y^2)^{1/2}.$$

We define another Cartesian system X',Y',Z' fixed with respect to the vector **H**, with Z' along **H** and with X' in the XY plane in such a way that Y' is below that plane when all settings are zero (Fig. 4). To find the components in X,Y,Z of a vector given in X',Y',Z' the vector has to be multiplied by the matrix **M**, given by

$$\mathbf{M} = \begin{pmatrix} \cos\varphi & -\sin\varphi\sin\chi & -\sin\varphi\cos\chi \\ \sin\varphi & \cos\varphi\sin\chi & \cos\varphi\cos\chi \\ 0 & -\cos\chi & \sin\chi \end{pmatrix}.$$

The columns are X', Y' and Z' expressed in X,Y,Z.

After setting φ and χ, **H** lies along Y, Y' is vertically downwards and X' coincides with X. This is seen in Fig. 5, where we look in the direction of $-Y$. When we increase ψ the vector **L** is seen rotating counter clockwise, by definition, in Fig. 5. This means that when **L** is vertical at $\psi = \psi_0$ (the best profile), it will be at the indicated position when $\psi = 0$, for in order to

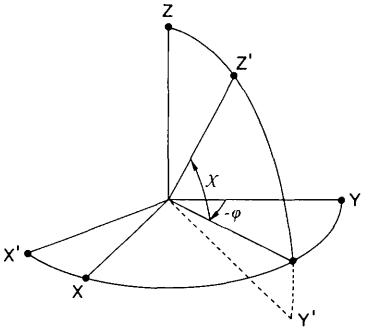

Fig. 4. The Cartesian coordinate system X,Y,Z is fixed to the eucentric point of the diffractometer. Z is vertical and X points to the source. The *values* of $-\varphi$ and χ are read in the sense of the arrows, the *settings* $-\varphi$ and χ are rotations in the opposite directions (CAD4 geometry). The Cartesian system X',Y',Z' is fixed to the crystal and different for a different **H**; the Z' axis is along **H**. The setting angle φ (negative, in this figure) brings X' to X and Z' into the YZ plane (rotation about Z). Then the setting angle χ brings Z' to Y (rotation about X).

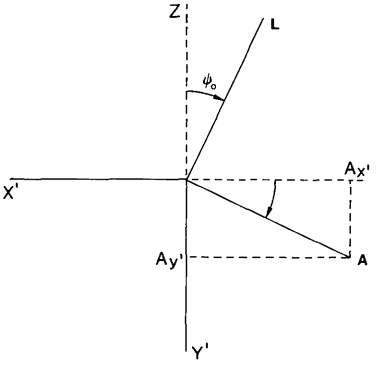

Fig. 5. Relative position of the Cartesian coordinate systems X,Y,Z (fixed to the diffractometer) and X',Y',Z' (fixed to the crystal with Z' along **H**) after setting φ and χ. The Y axis points to the viewer and **H** is along Y. The angle ψ_0, the azimuth for **L**, is *measured* in the sense of the arrow; the *rotation* ψ_0 brings **L** along Z, which is vertical. **L** and **A** are perpendicular to each other in this figure, as can be concluded from Fig. 2(*b*). $\tan \psi_0 = -A_{y'}/A_{x'}$; the minus sign because $A_{x'}$ is negative here and ψ_0 positive.

bring **L** vertical we have to increase ψ by ψ_0. This gives the components of **L** in X',Y',Z' as $(-\sin\psi_0, -\cos\psi_0, 0)$. Multiplication by **M** gives the expressions for L_x, L_y and L_z.

APPENDIX *B*

Seen along $-\mathbf{H}$, as in Fig. 5, the projection of **A** is perpendicular to **L**, as examination of Fig. 2(*b*) will show. The azimuth for **A** is therefore given by $\tan\psi_0 = -A_{y'}/A_{x'}$; the minus sign occurs because ψ_0 is by definition positive in this situation and $A_{y'}$ negative.

The components of **A** in X',Y',Z' are found from

$$\mathbf{A}_{X'Y'Z'} = \mathbf{M}^{-1}.\mathbf{A}_{XYZ},$$

where $\mathbf{M}^{-1} \equiv \mathbf{M}^T$, as **M** represents a pure rotation. Now the expression for $\tan\psi_0$ can be obtained.

References

ALEXANDER, L. E. & SMITH, G. S. (1962). *Acta Cryst.* **15**, 983–1004.

CLEGG, W. (1981). *Acta Cryst.* A**37**, 22–28.

GOLDSTEIN, H. (1959). *Classical Mechanics*, 6th ed., p. 143. Reading, MA & London: Addison-Wesley.

NELMES, R. J. (1975). *Acta Cryst.* A**31**, 273–279.

PAULUS, E. F. (1975). *Acta Cryst.* B**31**, 1191–1193.

RIECK, G. D. (1971). *High Temp. High Pressures.* **3**, 419–424.

TICHÝ, K. & BENEŠ, J. (1977). *Helv. Phys. Acta*, **50**, 459–466.

TICHÝ, K. & BENEŠ, J. (1979). *J. Appl. Cryst.* **12**, 10–14.

Acta Cryst. (1983). A**39**, 216–224

The Standard Crystallographic File Structure

BY I. D. BROWN

Institute for Materials Research, McMaster University, Hamilton, Ontario, Canada L8S 4M1

(*Received* 2 *August* 1982; *accepted* 27 *September* 1982)

Abstract

This paper describes a file structure that has been developed by a joint working party of the Data and Computing Commissions of the International Union of Crystallography. It is intended as a standard that can be used by those wishing to transfer any type of crystallographic data from one laboratory or program system to another.

Introduction

With the increasing use of computers in all branches of crystallography it has become necessary to define a standard file structure that will allow data files produced in one laboratory to be read directly into programs in a different laboratory.

At the Warsaw Congress of the International Union of Crystallography in 1978, the Data and Computing Commissions of the Union appointed a working party to propose a standard file structure for crystallographic data. The working party submitted its report at the 1981 Congress of the Union in Ottawa. This report, which is given below, was adopted by the Commissions with a recommendation to all authors of crystallographic programs that they write their programs so that they can read and write files with this structure.

Early in its deliberations the working group defined the following criteria to be met by the file structure. They are listed in decreasing order of importance.

1. *The file structure must be extendable to include all types of crystallographic data.*

2. *It must be compatible with current and future methods of data transmission.* Currently magnetic tapes are favoured with punch cards still sometimes used. Almost certainly there will be great changes in data transmission technology in the next few years.

3. *It should be easy to program for both reading and writing.* Files written in this structure are designed for machine-to-machine communication. Not all users will be experienced programmers or have access to large program systems. This implies the use of fixed formats. Users may well prefer to enter data in free format and use the computer to generate an exchange file in the standard form.

4. *The file should not require reread facilities* since these are not supported by all computers.

5. *A listing of a file written in this format should be easy to read visually* consistent with 3 above.

6. *The only records that must be included are those required for data management* (*e.g. END*). A standard crystallographic file will contain information of use to the writer and reader of the file. An author sending structural data to a journal will be interested in different

0567-7394/83/020216-09$01.50